arXiv:1606.00851v2 [cond-mat.mes-hall] 6 Jun 2016

Extracting inter-dot tunnel couplings between few donor quantum dots in silicon

S. K. Gorman, M. A. Broome, J. G. Keizer, T. F. Watson, S. J. Hile, W. J. Baker, M. Y. Simmons

Centre of Excellence for Quantum Computation and Communication Technology, School of Physics, University of New South Wales, Sydney, New South Wales 2052, Australia

(Dated: June 7, 2016)

The long term scaling prospects for solid-state quantum computing architectures relies heavily on the ability to simply and reliably measure and control the coherent electron interaction strength, known as the tunnel coupling, t_c. Here, we describe a method to extract the t_c between two quantum dots (QDs) utilising their different tunnel rates to a reservoir. We demonstrate the technique on a few donor triple QD tunnel coupled to a nearby single-electron transistor (SET) in silicon. The device was patterned using scanning tunneling microscopy-hydrogen lithography allowing for a direct measurement of the tunnel coupling for a given inter-dot distance. We extract t_c=5.5±1.8 GHz and t_c=2.2±1.3 GHz between each of the nearest-neighbour QDs which are separated by 14.5 nm and 14.0 nm, respectively. The technique allows for an accurate measurement of t_c for nanoscale devices even when it is smaller than the electron temperature and is an ideal characterisation tool for multi-dot systems with a charge sensor.

The entanglement of multiple quantum particles is becoming an established practice for enhanced measurement protocols in quantum metrology[1], secure communications in quantum key distribution[2,3] and is the central tenant of quantum computation[4]. Entanglement is created by a coherent coupling between quantum particles. In solid-state architectures, the spin-spin interaction between single electrons isolated to quantum dots (QDs) enables multi-qubit operations needed for universal quantum computation[5]. The strength of this interaction is governed by the coherent tunnel coupling term, t_c between two electron charge states of neighbouring QDs[6].

Unlike in conventional QD architectures where electrons are confined using metallic surface gates, donor based systems rely on the attractive Coulomb potential of the donor atoms themselves[7–11]. Nanoelectronic devices based on phosphorus doped silicon (Si:P) have recently demonstrated electron transport at the few electron level where spin-spin interactions can be observed[12–14]. Following this, the singlet-triplet states of a strongly coupled donor pair have been readout[15] and electrons confined to double QDs formed from donor clusters have been investigated using charge-sensing[16]. Importantly, for the scalability of multi-donor systems in a quantum computing architecture, the ability to simply and reliably measure t_c between donors is vital.

Unlike gate defined QDs[17–19], the value of t_c between isolated phosphorus donors or clusters in Si:P qubit architectures is fixed by the physical distance between the donors[20–22], and is difficult to tune using external gates since the donors are only separated by tens of nanometres[7,13,23]. Therefore, knowledge of t_c as a function of donor separation is extremely important for the design, fabrication, and operation of donor based qubits[20–22,24]. Several methods to determine t_c based on electron transport[25–28], spin funnel experiments[29,30] and the response of a quantum point contact across an inter-dot charge transition[17] have already been established. However, these techniques either require multiple-electron spin readout at low magnetic fields[29] or a large capacitive difference between the QDs and charge sensor[17]. The second condition requires that both QDs are at vastly different distances to the charge sensor; which is not ideal for single electron spin readout since complex shuttling protocols must be developed to determine the individual spin states.

In this letter we demonstrate a new method to determine t_c between QDs based on a simple time-resolved charge sensing technique. We use our method to determine t_c between adjacent QDs in a triple QD device that uses a single-electron transistor (SET) as a charge sensor. SETs have been used extensively for charge sensing in Si:P where they can perform high-fidelity single-electron spin readout[11,31–33]. We show how our time-resolved SET charge sensing technique can be used to determine t_c and at the same time allows for the extraction of electron temperature, T_e. The gate lever arms, α, can also be measured without the possibility of artificial broadening of the SET Coulomb blockade peaks[34] present in previously reported methods[31].

The device, shown in Fig. 1, was fabricated using a scanning tunneling microscope (STM) to selectively remove hydrogen from a passivated Si(100) 2×1 reconstructed surface. The lithographic mask is subsequently dosed with PH_3 and annealed to incorporate P atoms into the silicon substrate[35]. The lithographic outline of the device is shown in Fig. 1a,b. The QDs, L, M, and R (left, middle, and right) are formed with ∼5 P donors in each QD, determined by examining the size of the lithographic patches[11,13]. Three gates, G_L, G_M and G_R control the electron numbers on the QDs. The electrons are able to tunnel to a SET island used as the charge sensor. The SET is defined as a much larger QD in between source and drain leads with a control gate G_{SET}. It is operated with a source-drain bias of 0.3 mV and has a charging energy of ∼5 meV.

In our experiment, G_L and G_R are used to detune QDs L and R with respect to the SET, while G_M is

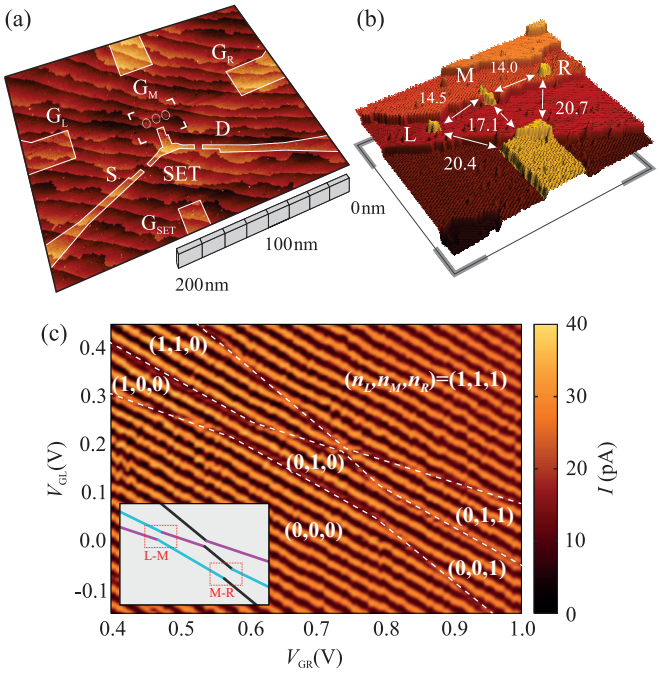

FIG. 1: A ∼5 donor triple quantum dot in Si:P with an adjacent singlet-electron transistor used as a charge sensor (all distances are in nm). (a) A scanning tunneling micrograph showing the lithographic outline of the device before PH_3 dosing. The device consists of four control gates (G_L, G_M, G_R, G_{SET}), a SET with source (S) and drain (D) leads, and three small QDs tunnel coupled to the SET. (b) A close-up of the three QDs. From the lithographic area it is estimated that they will contain ∼5 P donors. Neighbouring QDs are separated by 14.5 nm and 14.0 nm for the left-middle and middle-right, respectively. (c) The current through the SET as a function of the voltage on G_L and G_R. The breaks in the SET Coulomb blockade peaks show where the QD electrochemical potentials align with the SET and hence where a charge transition of the QD will occur. By following the SET breaks the typical pentagon structure of a triple QD can be seen, where the equivalent charge numbers are given by (n_L, n_M, n_R). The inset shows a schematic of the quadruple point with two dotted red boxed indicating the inter-dot transitions investigated in this work.

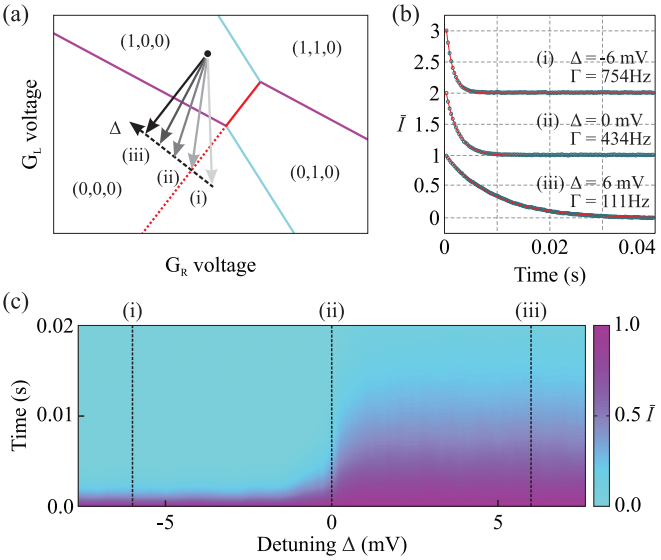

FIG. 2: Protocol for measurement of the inter-dot tunnel coupling utilising the difference in tunnel rates of the QDs to the SET. (a) A schematic of the L-M inter-dot transition showing the gate pulses required to measure the inter-dot tunnel coupling. The measurement protocol begins by loading an electron onto the left QD so that the system is in the (1,0,0) charge state. The gates are then pulsed adiabatically with respect to t_c but faster than the tunnel rate to the SET to move into the (0,0,0) state. The solid arrow shows the start and end point of a two level pulse to load and unload an electron from the (1,0,0)→(0,0,0). The dashed arrow shows the detuning, Δ for the unload phase of the two-level pulse; it sweeps past the inter-dot transition, marked by the red dashed line. (b) The normalised SET current, $\bar{I}$ showing the tunnel time, Γ(Δ) for different positions of detuning, Δ (the curves are offset by 1). (c) The normalised current map across the L-M charge transition showing the tunnel rate, Γ(Δ) as a function of Δ across the inter-dot transition.

used as global gate to shift the potential of the QDs. Figure 1c shows the SET transport current as a function of G_L and G_R. Enhanced current lines running at ∼45° due to Coulomb blockade of the SET can be seen with breaks corresponding to charge transitions of the three QDs. Due to the different capacitive coupling of the gates to the QDs, three lines of SET breaks with distinct slopes are visible. In addition a characteristic pentagon structure associated with the quadruple point of a triple QD[14,36,37] can be seen, confirming the presence of three separate QDs. We note that the absolute electron number has not been determined for this device; however, for the purpose of this work we assign the charge states shown in Fig. 1c where (n_L, n_M, n_R) represents the relative electron numbers on QDs L, M and R, respectively.

Next, we describe the method of determining t_c using the L-M transition as an example, see Fig. 2. The protocol involves measuring the tunnel rate from the QDs to the SET across an inter-dot transition, Fig. 2a. From the detuning dependency of the measured tunnel rates, the t_c can be extracted. Using a two level pulse scheme, the system is first initialised in the equivalent single electron state, (1,0,0) after which the second pulse moves into the (0,0,0) to unload this electron. This pulse duration, $t_p = 0.1$ ms, is adiabatic with respect to t_c but faster than either of the independent tunnel rates from the QDs to the SET. An exponential decay is fitted to the average current trace (200 cycles) and a tunneling rate Γ(Δ) extracted accordingly, see Fig. 2b. The protocol involves varying the unload point along a detuning axis, Δ across the inter-dot transition L-M and measuring the SET current $I_{SET}(t)$ as a function of time, shown in Fig. 2c. The procedure for the M-R transition is the

same; however, the initial charge configuration is chosen to be (0,0,1).

Far from the inter-dot transition at points (i) and (iii) in Fig. 2a the tunnel rate γ_L=$\Gamma(\Delta$=−6 mV)=111 Hz and γ_M=$\Gamma(\Delta$=6 mV)=754 Hz, respectively. However, as the unload point moves closer toward the inter-dot transition (shown by the dashed red line in Fig. 2a) $\Gamma(\Delta)\neq\gamma_L$ or γ_M and is given instead by the expression,

$$\Gamma(\Delta) \approx \sum_{i=L,M} P_i \Gamma_i, \tag{1}$$

where P_i is the probability of the electron occupying QD i=L, M and Γ_i is the effective tunnel rate which takes into account assisted tunneling via a neighbouring QD to the SET. Importantly both the occupation probabilities and effective tunnel rates will depend on the parameters, Δ, t_c and temperature of the system, T[17]. We have also performed numerical calculations based on a Linblad master equation approach and achieve the same form for the tunnel rate, $\Gamma(\Delta)$ (see appendix).

To find the general expression of $\Gamma(\Delta)$ we must compute the probabilities P_i of the electrons occupying the QDs in Eq. (1). Assuming that the QDs are in thermal contact with the SET with a temperature, T, since $k_BT \gg \gamma_i$[38], the probabilities of finding the electron in either of the two QDs is given by[17],

$$P_{\left\{\begin{smallmatrix} L \\ M \end{smallmatrix}\right\}} = \frac{1}{2} \pm \frac{\Delta \tanh\left(\frac{\theta}{2k_BT}\right)}{2\theta}, \tag{2}$$

where θ=$\sqrt{\Delta^2 + t_c^2}$, see Fig. 3a.

The shape of the (1,0,0)-(0,1,0) anti-crossing as a function of detuning, Δ dictates that the rates Γ_i follow a Lorentzian given by[33],

$$\Gamma_i = \gamma_i - \frac{\delta\gamma_{i,j} t_c^2}{2(\Delta^2 + t_c^2)}, \tag{3}$$

where $\delta\gamma_{i,j}$=γ_i−γ_j, see Fig. 3b. This means that at Δ=0 the effective tunnel rates are equal, Γ_L=Γ_M=$(\gamma_L$+$\gamma_M)/2$=$\bar{\gamma}_{LM}$, because the electron is fully delocalised over both QDs. In this analysis we have neglected the many excited states of the SET (that form a quasi-continuum) since the large detuning of the unload position makes the QD chemical potentials much higher than the SET Fermi level. This means the excited state energy levels are small compared to the overall energy scale. In addition, in the experiment we ensure that the unload position always follows the same Coulomb peak of the SET such that the same number of electrons are present on the SET.

Substituting Eq. (2) and (3) into Eq. (1) we find,

$$\Gamma(\Delta) \approx \bar{\gamma}_{LM} + \frac{\Delta^3(\delta\gamma_{LM}) \tanh\left(\frac{\theta}{2k_BT}\right)}{2\theta(\Delta^2 + t_c^2)}. \tag{4}$$

Figure 3 shows the functional forms of Γ_L and Γ_M, P_L and P_M, and $\Gamma(\Delta)$ as a function of detuning and for a fixed temperature (T=200 mK) and tunnel coupling (t_c=3.5 GHz). In Fig. 3c, the red dashed line corresponding to $\Gamma(\Delta)$ shows a plateau around Δ=0, where Γ_L=Γ_M. The width of the plateau is directly related to the strength of t_c. We can eliminate the possibility that the plateau is caused by an external charge fluctuation by looking at the stability map, Fig. 1c. There is no charge offset in the SET current that can be attributed to external charge movement. Equation 4 diverges from the theoretically predicted results using the Lindblad formalism for $t_c \gg k_BT$ where the sequential tunneling approach cannot be used.

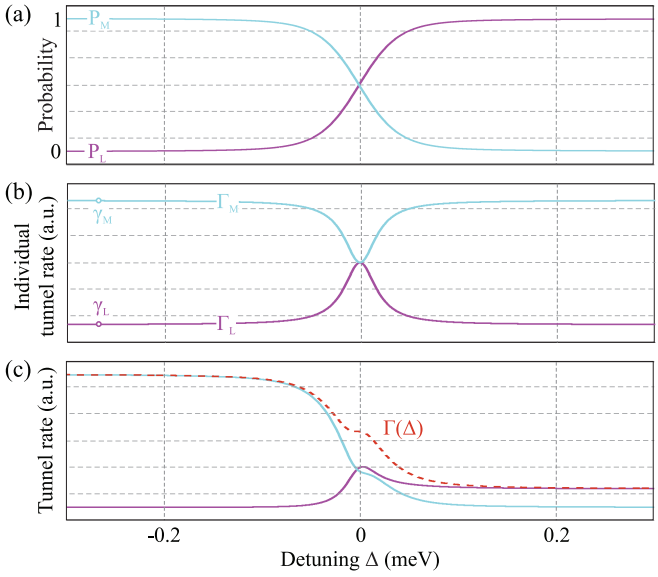

FIG. 3: Theoretical lineshape of the tunnel rates near the inter-dot transition. (a) The theoretical probability of an electron residing in each QD as a function of Δ at a temperature of T=200 mK. (b) The predicted effective tunnel rate to a SET for two tunnel coupled quantum dots (QDs) with t_c=3.5 GHz. At zero detuning, Δ=0 the tunnel rates to the SET must be equal since the electron is delocalised over both QDs. (c) Solid lines show the corresponding tunnel rates from each QD weighted by the electron occupation probability, *i.e.* the product of the traces shown in (a) and (b). The dashed line shows the sum of the weighted tunnel rates, $P_i\Gamma_i$, from Eq. (1), which theoretically predicts the form of the measured tunnel rate to the SET, $\Gamma(\Delta)$.

It is worth noting that if γ_L=γ_M, then $\Gamma(\Delta)$ does not vary as a function of Δ and our method cannot be used to gain any information about t_c. As a result, $\delta\gamma_{LM}\neq0$ is required which is most likely the case for any system, in particular for donor based QDs where the coupling decays exponentially with distance[20,21] meaning differences in donor position even on the atomic scale will change the tunnel rate significantly.

By fitting Eq. (4) to the tunnel rate across the transition we can determine t_c and the temperature, T. By varying the temperature we are able to determine both the minimum electron temperature, T_e as well as the lever

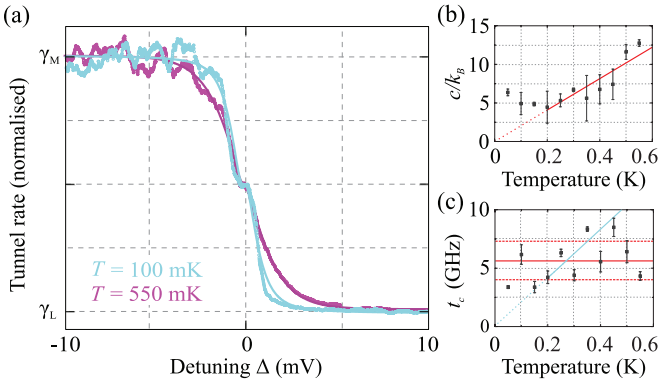

FIG. 4: Temperature dependence of $\Gamma(\Delta)$ for the lever arm calculation. (a) The temperature broadening effect of the tunnel rate, $\Gamma(\Delta)$ with a fit to Eq. (4). The plateau near zero detuning can be clearly seen at both T=100 mK and T=550 mK allowing for calculation of t_c at multiple temperatures. (b) The lever arm, α of the inter-dot transition can be found by repeating the measurement at various temperatures and plotting the fitting parameter, c/k_B. A fit to the section where c/k_B is linear (red solid line) gives α=0.0491±0.0028 as the inverse slope. The temperature at which c/k_B deviates from the linear fit is taken as the minimum T_e∼200 mK. (c) The experimentally determined tunnel coupling, t_c between L-M showing no temperature dependence. The solid red line shows the average tunnel coupling, with an error of one standard deviation given by the dashed lines. The blue solid line indicates the thermal energy k_BT demonstrating the measurement of t_c<k_BT for T≥300 mK.

arm for the inter-dot transition, α[31].

Figure 4a, shows the form of $\Gamma(\Delta)$ at two different temperatures T=100 mK and 550 mK where we see the impact of thermal broadening. The lever arm is related to the temperature, T by,

$$c = \frac{k_B T}{\alpha}, \tag{5}$$

where c is a fitting parameter used in place of k_BT in Eq. (4). By fitting a line to c/k_B as a function of temperature we can extract the lever arm from the inverse of the slope, $1/\alpha$ as in Fig. 4b. For the L-M transition we find α=0.0491±0.0028 and for the M-R transition α=0.0659±0.0142. The error in the M-R transition α is much larger compared to L-M transition α because the temperature dependence was not performed on this transition. Instead, the lever arm was determined by assuming a T_e=200 mK, calculated from the L-M transition temperature dependence in Fig. 4. The temperature at which c/k_B deviates from the linear fit is where T_e≠T and is taken as the minimum T_e of the system, here we find T_e∼200 mK.

Finally, from $\Gamma(\Delta)$ and α we can calculate t_c. For the L-M charge transition, we find t_c=5.5±1.8 GHz and for the M-R transition t_c=2.2±1.3 GHz. The technique allows t_c to be measured even when k_BT>t_c since the width of the plateau only depends on t_c. Therefore, t_c can also be measured as a function of temperature. The t_c should not have a temperature dependence since it corresponds to an energy separation. This is confirmed experimentally in Fig. 4c where t_c remains constant as the temperature is varied. The coherent coupling term between the QDs is much greater than the inelastic tunnel rate to the SET. This is a complex problem involving the shape of the electron wavefunctions in the SET and QDs, the crystallographic orientation, and the inelastic processes that gives rise to the tunnel event from the QD to the SET. We note that it is difficult to make a direct comparison to previously measured or theoretical results for single donors[20,21,24] since both the absolute electron and donor numbers are not known for our device. However, the t_c values obtained from this work are consistent with previously reported values with slightly different donor numbers and inter-dot distances[13,16].

In summary, we have demonstrated a relatively simple method to determine the tunnel coupling between adjacent QDs or donors that are tunnel coupled to a reservoir. The method can be applied to any system with a charge sensor where tunnel times can be measured and can also be used to obtain the minimum electron temperature and lever arms. The simplicity of the technique makes it ideal as a characterisation tool for future experiments examining multi-donor exchange interactions. Combining this method with atomic-precision lithography using a STM we can investigate the relationship between the inter-dot distance and the exchange coupling predicted from theoretical calculations[20,21,24].

This research was conducted by the Australian Research Council Centre of Excellence for Quantum Computation and Communication Technology (project no. CE110001027) and the US National Security Agency and US Army Research Office (contract no. W911NF-08-1-0527). M.Y.S. acknowledges an Australian Research Council Laureate Fellowship.

Appendix A: Numerical modelling of the tunnel rate across a double quantum dot

We model the system with a Hubbard-like Hamiltonian given by,

$$H = \sum_i (\epsilon_i - \mu_i) c_i^\dagger c_i + \sum_{i \neq j} \frac{t_{c(i,j)}}{2} (c_i^\dagger c_j + c_j^\dagger c_i), \tag{A1}$$

where, ϵ_i and μ_i are the detuning and chemical potential of QD i, c_i ($c_i^\dagger$) is the annihilation (creation) operator for the electron on QD i and $t_{c(i,j)}$ is the coupling term between the QDs. We assume that only 1 electron can be present in the system and work in the basis $\{|0\rangle, |L\rangle, |M\rangle\}$. To model the tunnel rates out of the QDs we assume that after the initial pulse from the (1,0,0) state to the unload position into the (0,0,0) the electron finds itself in an eigenstate of H at each value of detuning. This assumption is valid when the $t_{c(i,j)}$

is much greater than the tunnel rate out of either QD. Based on this assumption, the eigenstate of the system in the (0,0,0) will be given by,

$$\rho_g = \frac{1}{Z} e^{-H/k_B T}, \tag{A2}$$

with Z=Tr$(e^{-H/k_B T})$, k_B is Boltzmann's constant and T is the electron temperature. However, since we wait a time $t \gg T_2$ we let the off-diagonal terms in ρ_g go to zero. The inelastic tunnel rates for each QD are included by transforming the system from Hilbert space to Liouville space and assuming the Markov approximation[39]. In Liouville space the incoherent contribution is given by,

$$\mathcal{L}_\Gamma = \sum_i \frac{\Gamma_i}{2}(2c_i \otimes c_i - c_i^\dagger c_i \otimes \mathbb{I} - \mathbb{I} \otimes c_i^\dagger c_i), \tag{A3}$$

Finally, we solve the Lindblad equation as a function of the detuning across the anti-crossing between the two charge states,

$$\dot{\rho} = i(\mathbb{I} \otimes H - H \otimes \mathbb{I})\rho_g + \mathcal{L}_\Gamma \rho_g. \tag{A4}$$

We watch $\rho_{00}(t)$ during the time evolution. The time dependence of $\rho_{00}(t)$ will follow a double exponential decay due to the tunneling out of the states $|L\rangle$ and $|M\rangle$,

$$\rho_{00}(t) = 1 - \rho_{LL}(0)e^{-t\Gamma_L} - \rho_{MM}(0)e^{-t\Gamma_M}, \tag{A5}$$

where $\rho_{LL}(0)$ and $\rho_{MM}(0)$ are calculated from ρ_g. In the experiment we fit the decay to a single exponential, effectively taking a waited average of the double exponential decay. This is the origin of Eq. 1 in the main text. We find that the time when $\rho_{00}(t) = 1 - e^{-1}$ agrees well with Eq. 1 for most values of t_c and deviates in the limit that $k_B T/t_c \to 0$. However, the width of the plateau region, which is proportional to t_c remains valid for all values of $k_B T/t_c$.

[1] V. Giovannetti, S. Lloyd, and L. Maccone, Nature Photonics **5**, 222 (2011).
[2] W.-Y. Hwang, Phys. Rev. Lett. **91**, 057901 (2003).
[3] H.-K. Lo and H. F. Chau, Science **283**, 2050 (1999).
[4] D. DiVincenzo, arXiv:quant-ph/0002077v3 (2000).
[5] J. Levy, Phys. Rev. Lett. **89**, 147902 (2002).
[6] T. Takakura, A. Noiri, T. Obata, T. Otsuka, J. Yoneda, K. Yoshida, and S. Tarucha, Appl. Phys. Lett. **104**, 113109 (2014).
[7] B. E. Kane, Nature **393**, 133 (1998).
[8] M. Pierre, R. Wacquez, X. Jehl, M. Sanquer, M. Vinet, and O. Cueto, Nat. Nanotech. **5**, 133 (2009).
[9] M. Fuechsle, S. Mahapatra, F. A. Zwanenburg, M. Friessen, M. A. Eriksson, and M. Y. Simmons, Nature Nanotech. **5**, 502 (2010).
[10] G. Mazzeo, E. Prati, M. Belli, G. Leti, S. Cocco, M. Fanciulli, F. Guagliardo, and G. Ferrari, Appl. Phys. Lett. **100**, 213107 (2012).
[11] H. Buch, S. Mahapatra, R. Rahman, A. Morello, and M. Y. Simmons, Nature Commun. **4**, 2017 (2013).
[12] B. Roche, E. Dupont-Ferrier, B. Voisin, M. Cobian, X. Jehl, R. Wacquez, M. Vinet, Y.-M. Niquet, and M. Sanquer, Phys. Rev. Lett. **108**, 206812 (2012).
[13] B. Weber, Y. H. M. Tan, S. Mahapatra, T. F. Watson, H. Ryu, R. Rahman, L. C. L. Hollenberg, G. Kilmeck, and M. Y. Simmons, Nature Nanotech. **9**, 430 (2014).
[14] T. F. Watson, B. Weber, J. A. Miwa, S. Mahapatra, R. M. P. Heijen, and M. Y. Simmons, Nano Lett. **14**, 1830 (2014).
[15] J. P. Dehollain, J. T. Muhonen, K. Y. Tan, A. Saraiva, D. N. Jamieson, A. S. Dzurak, and A. Morello, Phys. Rev. Lett. **112**, 236801 (2014).
[16] T. F. Watson, B. Weber, H. Buch, M. Fuechsle, and M. Y. Simmons, Appl. Phys. Lett. **107**, 233511 (2015).
[17] L. DiCarlo, H. J. Lynch, A. C. Johnson, L. I. Childress, K. Crockett, C. M. Marcus, M. P. Hanson, and A. C. Gossard, Phys. Rev. Lett. **92**, 226801 (2004).
[18] J. R. Petta, A. C. Johnson, C. M. Marcus, M. P. Hanson, and A. C. Gossard, Phys. Rev. Lett. **93**, 186802 (2004).
[19] F. H. L. Koppens, J. A. Folk, J. M. Elzerman, R. Hanson, L. H. Williems van Beveran, I. T. Vink, H. P. Tranitz, W. Wegscheider, L. P. Kouwenhoven, and L. M. K. Vandersypen, Science **309**, 1346 (2005).
[20] B. Koiller, X. Hu, and S. Das Sarma, Phys. Rev. Lett. **88**, 027903 (2002).
[21] C. J. Wellard, L. C. L. Hollenberg, F. Pariosoli, L. M. Kettle, H.-S. Goan, J. A. L. McIntosh, and D. N. Jamieson, Phys. Rev. B **68**, 195209 (2003).
[22] L. C. L. Hollenberg, A. D. Greentree, A. G. Fowler, and C. J. Wellard, Phys. Rev. B **74**, 045311 (2006).
[23] A. J. Skinner, M. E. Davenport, and B. E. Kane, Phys. Rev. Lett. **90**, 087901 (2003).
[24] B. Koiller, X. Hu, and S. Das Sarma, Phys. Rev. B. **66**, 115201 (2002).
[25] Y. V. Nazarov, Physica B **189**, 57 (1993).
[26] F. R. Waugh, M. J. Berry, C. H. Crouch, C. Livermore, D. J. Mar, R. M. Westervelt, K. L. Campman, and A. C. Gossard, Phys. Rev. B **53**, 1413 (1996).
[27] W. G. van der Wiel, S. De Franceschi, J. M. Elzerman, T. Fujisawa, S. Tarucha, and L. P. Kouwenhoven, Rev. Mod. Phys. **75**, 1 (2003).
[28] E. Dupont-Ferrier, B. Roche, B. Voisin, X. Jehl, R. Wacquez, M. Vinet, M. Sanquer, and S. De Franceschi, Phys. Rev. Lett. **110**, 136802 (2013).
[29] J. R. Petta, A. C. Johnson, J. M. Taylor, E. A. Laird, A. Yacoby, M. D. Lukin, C. M. Marcus, M. P. Hanson, and A. C. Gossard, Science **309**, 2180 (2005).
[30] B. M. Maune, M. G. Borselli, B. Huang, T. D. Ladd, P. W. Deelman, K. S. Holabird, A. A. Kiselev, I. Alvarado-Rodriguez, R. S. Ross, A. E. Schmitz, et al., Nature **481**, 344 (2012).
[31] A. Morello, J. J. Pla, F. A. Zwanenburg, K. W. Chan, K. Y. Tan, H. Huebl, M. Mottonen, C. D. Nugroho, C. Yang, J. A. van Donkelaar, et al., Nature **467**, 687 (2010).
[32] J. J. Pla, K. Y. Tan, J. P. Dehollain, W. H. Lim, J. J. L. Morton, D. N. Jamieson, A. S. Dzurak, and A. Morello,

Nature **489**, 541 (2012).
[33] T. F. Watson, B. Weber, M. G. House, H. Buch, and M. Y. Simmons, Phys. Rev. Lett. **115**, 166806 (2015).
[34] B. Kung, C. Rossler, M. Beck, J. Faist, T. Ihn, and K. Ensslin, New J. Phys. **14**, 083003 (2012).
[35] A. Fuhrer, M. Fuechsle, T. C. G. Reusch, B. Weber, and M. Y. Simmons, Nano Lett. **9**, 707 (2009).
[36] M. Busl, G. Grainger, L. Gaudreau, R. Sanchez, A. Kam, M. Pioro-Ladriere, S. A. Studenikin, P. Zawadzki, Z. R. Wasilewski, A. S. Sachrajda, et al., Nature Nano. **8**, 261 (2013).
[37] F. R. Braakman, P. Barthelemy, C. Reichl, W. Wegscheider, and L. M. K. Vandersypen, Nature Nano. **8**, 432 (2013).
[38] M. G. House, T. Kobayashi, B. Weber, S. J. Hile, T. F. Watson, J. van der Heijden, S. Rogge, and M. Y. Simmons, Nat. Commun. **6**, 8848 (2015).
[39] S. K. Gorman, M. A. Broome, W. J. Baker, and M. Y. Simmons, Phys. Rev. B **92**, 125413 (2015).